Fake symmetry transitions in lattice Dirac spectra

M. Schnabel[1] and T. Wettig[2]
[1] *Institut für Theoretische Physik, Universität Regensburg, D-93040 Regensburg, Germany*
[2] *Center for Theoretical Physics, Yale University, New Haven, CT 06520-8120*
(printed February 1, 2008)

In a recent lattice investigation of Ginsparg-Wilson-type Dirac operators in the Schwinger model, it was found that the symmetry class of the random matrix theory describing the small Dirac eigenvalues appeared to change from the unitary to the symplectic case as a function of lattice size and coupling constant. We present a natural explanation for this observation in the framework of a random matrix model, showing that the apparent change is caused by the onset of chiral symmetry restoration in a finite volume. A transition from unitary to symplectic symmetry does not occur.

PACS numbers: 11.15.Ha, 12.38.Gc, 05.45.Pq

I. INTRODUCTION

In the past two years, Dirac operators $\mathcal{D}$ satisfying the Ginsparg-Wilson (GW) condition [1],

$$\mathcal{D}\gamma_5 + \gamma_5\mathcal{D} = 2\mathcal{D}\gamma_5 R\mathcal{D}\,, \tag{1}$$

have attracted a great deal of attention in the lattice community because of their vastly improved chiral and topological properties. In a recent lattice study of the Schwinger model, Farchioni et al. [2] investigated two different versions of $\mathcal{D}$, a fixed point Dirac operator $\mathcal{D}_{\rm fp}$ [3] and Neuberger's Dirac operator $\mathcal{D}_{\rm Ne}$ [4]. For the purpose of the present study, these two operators have essentially identical properties, and we concentrate on $\mathcal{D}_{\rm Ne}$ in the following. The subtracted lattice condensate is defined by [4,3]

$$\langle\bar\psi\psi\rangle_{\rm sub} = -\frac{1}{V}\left\langle \mathrm{tr}\,\tilde{\mathcal{D}}^{-1}\right\rangle_{\rm gauge}\,, \tag{2}$$

where $\tilde{\mathcal{D}} = \mathcal{D}(1-R\mathcal{D})^{-1}$ and V is the physical volume. The operator $\tilde{\mathcal{D}}$ shares some important features with the continuum Dirac operator in Euclidean space. It is anti-Hermitian and satisfies $\{\tilde{\mathcal{D}},\gamma_5\} = 0$. Thus, its nonzero eigenvalues occur in pairs $\pm i\lambda_n$ with λ_n real. The spectral density of $i\tilde{\mathcal{D}}$ is defined by $\rho(\lambda) = \langle\sum_n(\lambda-\lambda_n)\rangle/V$. The Banks-Casher relation [5] then reads

$$\Sigma \equiv -\lim_{V\to\infty}\langle\bar\psi\psi\rangle_{\rm sub} = \lim_{\lambda\to 0}\lim_{V\to\infty}\pi\rho(\lambda)\,, \tag{3}$$

where it is important that the thermodynamic limit is taken first.

Our main concern in the present work are the somewhat puzzling observations made in Ref. [2] where the spectral properties of $\tilde{\mathcal{D}}$ were compared to predictions of chiral random matrix theory (RMT) [6]. RMT is a simple model which yields exact analytical results for the spectral correlations of the Dirac operator on the scale of the mean level spacing. Because of the chiral structure of the problem, one has to distinguish two regions in the spectrum, (i) the bulk and (ii) the eigenvalues in the vicinity of zero (the latter is called the microscopic region or the hard edge of the spectrum). The analytical predictions of RMT are different in these two regions. Furthermore, there are three different symmetry classes, the chiral orthogonal (chOE), unitary (chUE), and symplectic (chSE) ensembles [7].

Let us briefly summarize those findings of Ref. [2] which are of relevance to the present work. The Schwinger model (QED_2) is in the symmetry class of the chUE. For large volumes $V \propto L^2/\beta$ (L is the number of lattice sites in each dimension and $\beta = 1/(ea)^2$ is the dimensionless coupling), it was found that the bulk as well as the hard edge of the spectrum are nicely described by the chUE predictions. As V decreases, the bulk properties are still given by the chUE whereas at the hard edge, the data suggest a transition to chSE behavior. In Ref. [2], the sectors of topological charge $\nu = 0$ and $\nu = 1$ were investigated, and the apparent transition was seen in both sectors. These observations are puzzling, since it is not clear where the symplectic symmetry should come from. Also, the spectrum is not doubly degenerate as expected for the chSE. The authors of Ref. [2] already suggested that their observation might be an artifact of the small physical volume and that the agreement with the chSE may be accidental.

In the framework of RMT, a transition between the two symmetry classes can be described by the simple model

$$(1-\alpha)\,\mathcal{D}_{\rm chUE} + \alpha\,\mathcal{D}_{\rm chSE} \tag{4}$$

with Dirac operators of the appropriate symmetries and $0 \le \alpha \le 1$ interpolating between the two ensembles. However, in such a model the transition from chUE to chSE is expected to occur simultaneously in the bulk and in the microscopic domain. We have confirmed this expectation numerically. Thus, the simple ansatz (4) cannot explain the findings of Ref. [2]. This is as it should be, since we do not expect a symplectic symmetry to be present in the first place.

For RMT to be applicable at the hard edge, it is necessary that chiral symmetry is spontaneously broken, i.e., we require $\rho(0) > 0$. (Since on the lattice one is always

working at finite volume, we mean here the value obtained by extrapolating $\rho(\lambda)$ many level spacings away from zero to $\lambda = 0$.) As we shall see, the apparent transition from chUE to chSE symmetry in the microscopic domain is caused by the fact that $\rho(0)$ vanishes as the physical volume decreases. This will be shown in more detail below, using a random matrix model which we construct in the following section. The spectral properties we consider are introduced in Sec. III, our results are presented and discussed in Sec. IV, and conclusions are drawn in Sec. V.

II. THE RANDOM MATRIX MODEL

Our approach closely parallels the construction of the Neuberger operator [4]. The Wilson Dirac operator for the $d = 2$ dimensional Schwinger model defined on an $L \times L$ lattice reads

$$\mathcal{M}_{x,y} = \delta_{x,y} - \kappa \sum_{\mu=1}^{2} \big[(1-\sigma_\mu) U_\mu(x) \Delta_{x,y-\hat{\mu}} + (1+\sigma_\mu) U_\mu^\dagger(x-\hat{\mu}) \Delta_{x,y+\hat{\mu}}\big] \quad (5)$$

with hopping parameter $\kappa = 1/(2m+4)$ and Pauli matrices σ_i. As in Ref. [2], we will restrict ourselves to the case $m = -1$, $\kappa = 1/2$. The boundary conditions for the fermions are periodic in space and anti-periodic in Euclidean time. This is taken into account by the function $\Delta_{x,y\pm\hat{\mu}}$ which is the usual Kronecker delta $\delta_{x,y\pm\hat{\mu}}$ except for the links from $x_2 = L$ to $x_2 = 1$ for which there is an extra factor of -1. The U(1) gauge fields are represented by $2L^2$ phases $U_\mu(x)$ which obey periodic boundary conditions and fluctuate in the update process. In our model, they are simply replaced by independent uncorrelated random phases $\exp(i\varphi)$ with φ drawn at random from the interval $[-\delta, \delta]$. For a single flavor with two spinor indices, $\mathcal{M}$ thus becomes a (sparse) random matrix of dimension $2L^2$.

From the matrix $\mathcal{W}$ obtained by replacing the gauge fields by random phases we construct the Neuberger operator [4],

$$\mathcal{W}_{\rm Ne} = \mathbb{1} + \gamma_5\, \varepsilon(\gamma_5 \mathcal{W})\,, \quad (6)$$

where ε is the sign function $\varepsilon(A) \equiv A/\sqrt{AA^\dagger}$. $\mathcal{D}_{\rm Ne}$ (and hence also $\mathcal{W}_{\rm Ne}$) satisfies the GW condition (1) with $R = 1/2$. Its spectrum is located on the unit circle in the complex plane with center at $z = 1$. Furthermore, for certain background fields it possesses exact zero modes whose number is related to the topological charge of the background field. In analogy with the definition of $\tilde{\mathcal{D}}$ we finally construct the random matrix

$$\widetilde{\mathcal{W}} = \mathcal{W}_{\rm Ne}(1 - \mathcal{W}_{\rm Ne}/2)^{-1}\,. \quad (7)$$

This projects the spectrum of $\mathcal{W}_{\rm Ne}$ onto the imaginary axis. In the following, we will investigate the spectrum of the matrix $\widetilde{\mathcal{W}}$.

There are two parameters in the random matrix model, the linear lattice size L and the width 2δ of the distribution $P(\varphi) = \theta(\delta+\varphi)\theta(\delta-\varphi)/2\delta$. The parameter δ is restricted to the interval $0 \le \delta \le \pi$. It models the coupling β used in the lattice gauge simulation. Small values of δ correspond to phases $\exp(i\varphi)$ which fluctuate only weakly around unity. Thus, small values of δ correspond to large values of β and vice versa.

An analytical treatment of the problem is very difficult. Therefore, we performed a numerical study for several combinations of the parameters L and δ. As we shall see, the random matrix model is able to reproduce and to explain the findings of Ref. [2].

III. SPECTRAL PROPERTIES

Since our main purpose in this work is to understand the puzzling observations of Ref. [2], we have investigated the same quantities considered therein. These are the spectral density $\rho(\lambda)$, the distribution of the smallest (positive) eigenvalue $P(\lambda_{\rm min})$, and the nearest neighbor spacing distribution $P(s)$. The quantity s is the spacing between adjacent eigenvalues in the bulk after the spectrum has been unfolded [8]. $P(\lambda_{\rm min})$ and $P(s)$ measure the spectral properties at the hard edge and in the bulk of the spectrum, respectively. (We will not discuss the microscopic spectral density which was also considered in Ref. [2] since for the purpose of the present study, $P(\lambda_{\rm min})$ is sufficient to reveal the properties of the spectrum near $\lambda = 0$.) The global density $\rho(\lambda)$ of the random matrix model is not a universal quantity, i.e., it depends on the details of the model and is not expected to agree with real lattice data. However, $P(\lambda_{\rm min})$ and $P(s)$ are universal for a specific symmetry class, i.e., these functions are insensitive to the details of the dynamics, and the results obtained in RMT should agree with those of lattice simulations (unless the conditions are such that RMT is not applicable, see below).

The nearest neighbor spacing distribution $P(s)$ in the bulk of the spectrum is expected to agree with the RMT result irrespective of whether or not chiral symmetry is broken [9]. In other words, it is insensitive to the value of $\rho(0)$. $P(s)$ can be unambiguously constructed from the lattice data without any free parameter by unfolding. The RMT results for $P(s)$ are well approximated by the Wigner surmise [8]

$$P(s) = \begin{cases} (32/\pi^2)\, s^2 \exp\left(-4s^2/\pi\right) & \text{chUE} \\ (2^{18}/3^6\pi^3)\, s^4 \exp\left(-64 s^2/9\pi\right) & \text{chSE}\,. \end{cases} \quad (8)$$

The nearest neighbor spacing s is expressed in units of the mean level spacing in the bulk. Note that $P(s)$ does not depend on ν or on the number of massless flavors N_f.

In contrast to $P(s)$, $P(\lambda_{\rm min})$ is only given by the RMT result if chiral symmetry is broken, i.e., if $\rho(0) \neq 0$. Also

in contrast to $P(s)$, it depends on the number of zero modes ν and on N_f. In the following, we restrict ourselves to the quenched case, $N_f = 0$. The energy scale for a comparison between the RMT result and numerical data is set by the mean level spacing at the hard edge, $1/V\rho(0) = \pi/V\Sigma$, which can be determined by Eq. (3) without resorting to RMT. In terms of the variable $z = V\Sigma\lambda_{\rm min}$, the RMT results for the chUE are given by [10]

$$P(z) = \begin{cases} (z/2)\, e^{-z^2/4} & \nu = 0, \\ (z/2)\, e^{-z^2/4}\, I_2(z) & \nu = 1, \\ (z/2)\, e^{-z^2/4} \left[I_2^2(z) - I_1(z) I_3(z) \right] & \nu = 2, \end{cases} \quad (9)$$

where I denotes the modified Bessel function. The RMT results for the chSE are more complicated and can be found in Ref. [11]. The only simple case is $\nu = 0$ for which [12]

$$P(z) = \sqrt{\pi/2}\, z^{3/2}\, e^{-z^2/2}\, I_{3/2}(z)\,. \quad (10)$$

As we shall show in Sec. IV, the apparent change from chUE to chSE symmetry in $P(\lambda_{\rm min})$ is caused by the fact that $\rho(0)$ (i.e., the extrapolated value) vanishes in a finite volume for sufficiently weak coupling. An unambiguous and parameter-free comparison of numerical data with RMT results is only possible if $\rho(0)$ and hence Σ are nonzero. In the present work, however, we are particularly concerned with the region in the parameter space (L, δ) where $\Sigma \to 0$. In this case, we are faced with the problem of how to set the energy scale for $\lambda_{\rm min}$. We circumvent this problem by employing three independent methods of analyzing the data.

(1) We rescale the smallest eigenvalue, both for the numerical data and for the RMT results, such that $\langle \lambda_{\rm min} \rangle = 1$. In this way, the various cases we consider are characterized only by the shape of the distribution; the ambiguity in the determination of the scale is avoided.

(2) For each data set, we construct the ratio

$$r = \frac{\langle \lambda_{\rm min} \rangle}{\sqrt{\langle \lambda_{\rm min}^2 \rangle - \langle \lambda_{\rm min} \rangle^2}} \quad (11)$$

which eliminates the energy scale. The RMT results for this ratio are

$$r = \begin{cases} 1.91306 & \text{chUE, } \nu = 0, \\ 2.78248 & \text{chSE, } \nu = 0, \\ 2.81978 & \text{chUE, } \nu = 1, \\ 4.07231 & \text{chSE, } \nu = 1, \\ 3.55611 & \text{chUE, } \nu = 2, \\ 5.11362 & \text{chSE, } \nu = 2. \end{cases} \quad (12)$$

(3) We fit the data for $P(\lambda_{\rm min})$ to the RMT results of both the chUE and the chSE (for fixed ν) and apply goodness-of-fit tests [13]. For the determination of the scale, we use the method of maximum likelihood. For the quality of the fit, we use three tests:
(3a) A Smirnov-Cramér-Von Mises test of the unbinned data (see Sec. 11.4.1 of Ref. [13]). This test yields a number NW^2 which for a good fit is smaller than one (N is the number of configurations).
(3b) A chi-square test of the binned data using equiprobable bins, with an "optimal" number k of bins scaling like $N^{2/5}$ (see Sec. 11.2.3 of Ref. [13]). For a good fit, the resulting $\chi^2/(k-1)$ is not much larger than one.
(3c) The probability Q that the chi-square should exceed the value of χ^2 computed in (3b) by chance [14]. This is given by $Q = 1 - P((k-1)/2, \chi^2/2)$ with the incomplete gamma function $P(a,x) = \int_0^x dt\, t^{a-1} e^{-t}/\Gamma(a)$. If the probability Q is very small, the theory can be statistically rejected.

Let us emphasize again that in the region where chiral symmetry is spontaneously broken, $P(\lambda_{\rm min})$ is unambiguously given by RMT without any free parameter. Here, however, we explicitly consider the transition region where $\rho(0) \to 0$. We use the somewhat more involved methods (1)-(3) to make clear and parameter-independent statements on the behavior of $P(\lambda_{\rm min})$ in this transition region.

IV. RESULTS AND DISCUSSION

We have scanned the parameters L and δ to reveal the main properties of the spectrum. For each parameter set we generated several thousand random matrices $\widetilde{\mathcal{W}}$ as described in Sec. II. For each realization the full spectrum was computed, and the configurations were grouped according to their number ν of zero modes. The quantities we consider were then averaged over realizations of $\widetilde{\mathcal{W}}$.

In Fig. 1, we have fixed the parameter $L = 10$ and varied the parameter δ. We have plotted the spectral density $\rho(\lambda)$ in the vicinity of $\lambda = 0$ for all ν combined, and the rescaled distribution of the smallest positive eigenvalue $P(\lambda_{\rm min})$ for $\nu = 0, 1, 2$. (Note that the zero modes are not included in $\rho(\lambda)$.) Also given in the figure are the values of the ratio r, see Eq. (11). The results of the goodness-of-fit tests (3a)-(3b) defined in Sec. III are summarized in Table I.

The main message of this paper can be read off immediately from these plots. The largest value of $\delta = 1.6$ corresponds to the strongest coupling and hence to the largest physical volume. The extrapolated value of $\rho(0)$ is clearly nonzero. Thus, RMT is applicable, and $P(\lambda_{\rm min})$ agrees very well with the chUE curves for all three values of ν. The data also pass the other tests proposed in Sec. III: The ratio r agrees well with that of the chUE, see Eq. (12), and the goodness-of-fit tests, see Table I, show that the chUE describes the data well.

On the other hand, the smallest value of $\delta = 1.2$ corresponds to the weakest coupling and hence to the smallest physical volume. In this case, the extrapolated value of

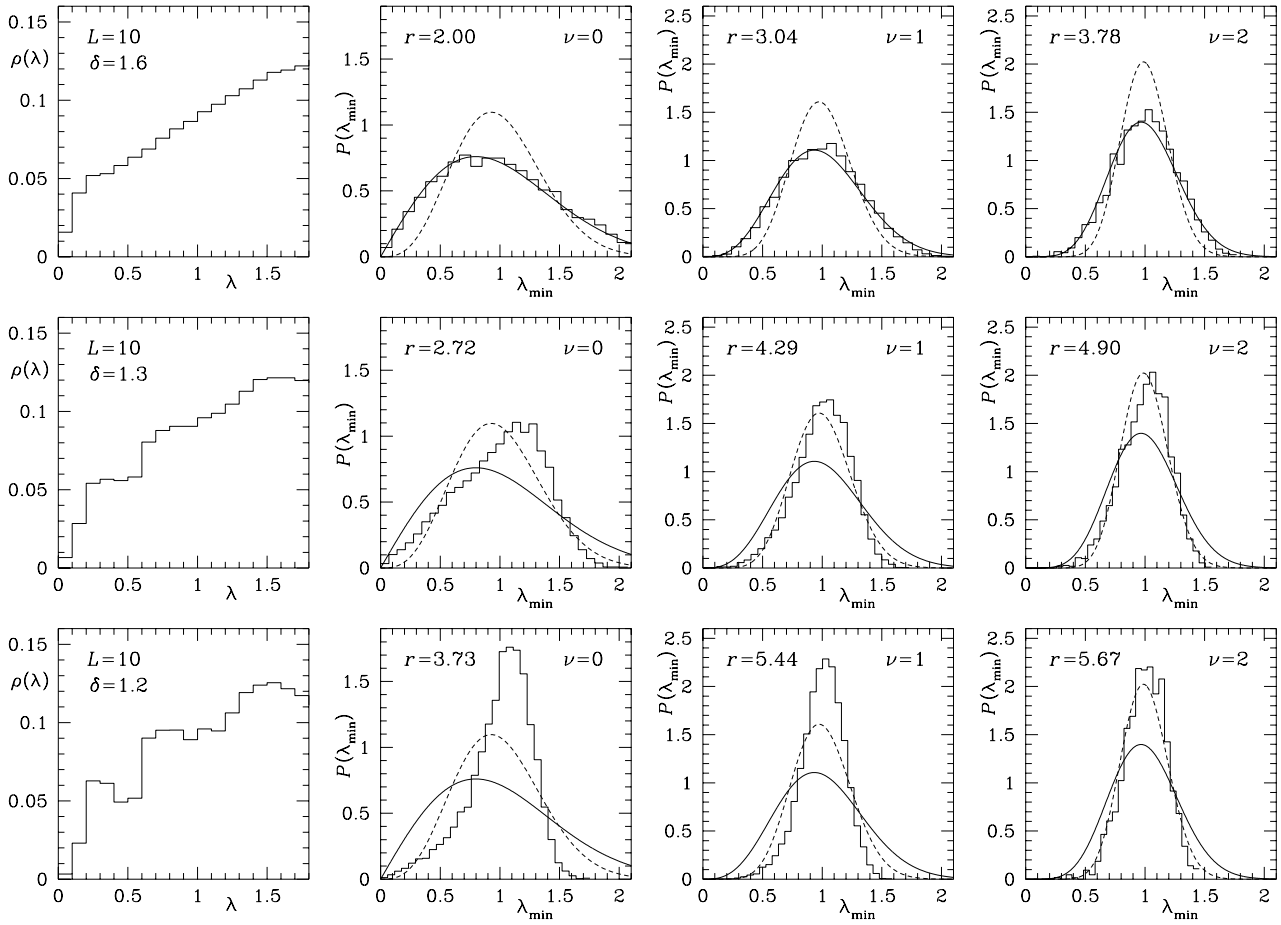

FIG. 1. Global spectral density $\rho(\lambda)$ (left column) and rescaled distribution of the smallest eigenvalue $P(\lambda_{\min})$ of $\widetilde{\mathcal{W}}$ for $L = 10$ as a function of δ for $\nu = 0, 1, 2$. The solid and dotted curves in the plots for $P(\lambda_{\min})$ are the chUE and chSE predictions, respectively. The quantity r is defined in Eq. (11).

$\rho(0)$ vanishes, and chiral symmetry is restored. Thus, a comparison with RMT becomes meaningless in the microscopic region. The shape of the distribution $P(\lambda_{\min})$ as well as the ratio r of Eq. (11) are now different from the RMT predictions. Neither the chUE nor the chSE provide good fits to the data, as can be seen from the goodness-of-fit tests in Table I. For the intermediate case of $\delta = 1.3$, the value of $\rho(0)$ is neither clearly zero nor clearly nonzero. Figure 1 and Table I indicate that already in this case RMT no longer provides a good description of the data.

Equivalent conclusions can be drawn from Fig. 2 in which we exhibit similar plots, but now for a fixed value of $\delta = \pi$ (corresponding to "strongest coupling") and L varied from 10 to 4. The goodness-of-fit tests are also shown in Table I. Again, as the physical volume decreases, the extrapolated value of $\rho(0)$ vanishes, and the agreement between numerical data and RMT breaks down. We also observe from Fig. 2 that RMT ceases to describe the data first for the nonzero values of ν and then for $\nu = 0$.

A remarkable fact, however, is that there are some combinations of the parameters L and δ for which the shape of the distribution $P(\lambda_{\min})$ resembles the chSE pre-

L	δ	ν	NW^2		χ^2		Q	
			chUE	chSE	chUE	chSE	chUE	chSE
10	1.6	0	0.674	25.2	1.29	14.0	0.073	10^{-126}
10	1.6	1	2.49	22.25	1.47	13.9	0.008	10^{-148}
10	1.6	2	1.36	9.48	2.55	9.52	10^{-8}	10^{-68}
10	1.3	0	62.8	11.7	37.6	11.8	0	10^{-126}
10	1.3	1	73.2	8.78	45.4	7.61	0	10^{-73}
10	1.3	2	11.3	1.34	9.05	3.22	10^{-56}	10^{-11}
10	1.2	0	290	103	179	67.5	0	0
10	1.2	1	145	39.4	108	29.2	0	0
10	1.2	2	12.1	1.23	7.68	3.26	10^{-37}	10^{-10}
10	π	0	0.109	36.8	1.37	17.4	0.033	10^{-176}
10	π	1	1.20	38.9	1.88	20.3	10^{-5}	10^{-254}
10	π	2	0.268	19.4	2.10	14.4	10^{-6}	10^{-131}
7	π	0	4.88	21.9	4.12	12.6	10^{-25}	10^{-127}
7	π	1	13.8	10.7	7.17	8.98	10^{-66}	10^{-90}
7	π	2	3.71	2.40	3.82	4.22	10^{-15}	10^{-18}
4	π	0	83.6	151	21.2	38.2	0	0
4	π	1	259	25.3	116	13.3	0	10^{-276}
4	π	2	16.6	4.97	14.0	7.14	10^{-75}	10^{-31}

TABLE I. Results of the goodness-of-fit tests as explained at the end of Sec. III. Zero means zero to machine precision.

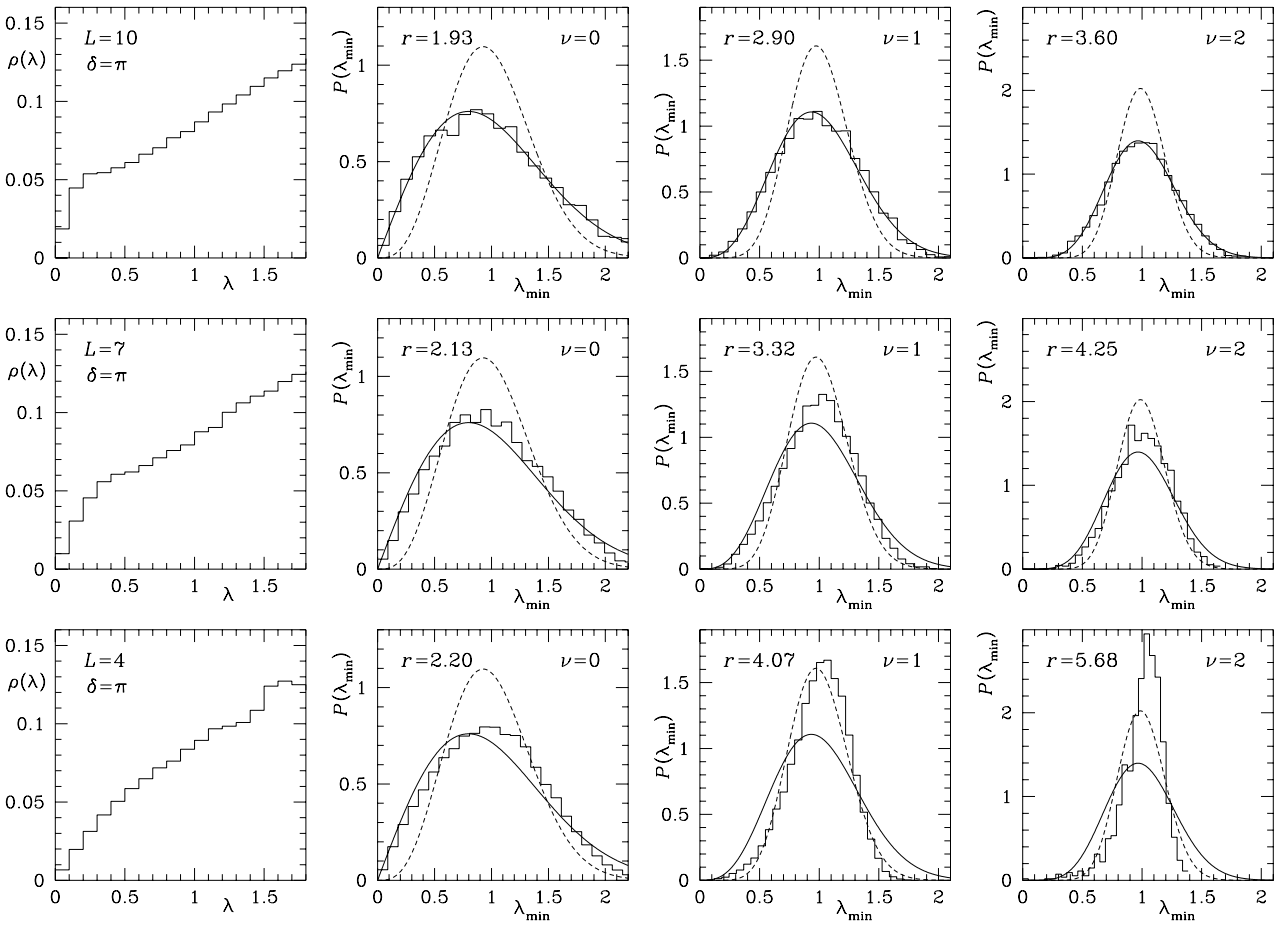

FIG. 2. Same as Fig. 1 but keeping $\delta = \pi$ fixed and varying L.

diction. This effect is particularly pronounced for the nonzero values of ν, which was also found in Ref. [2] (for $\nu = 1$). In our data, this is seen in Fig. 1 for $\delta = 1.3$, $\nu = 1, 2$ and $\delta = 1.2$, $\nu = 2$, respectively, and in Fig. 2 for $L = 4$, $\nu = 1$. (Recall that the plots of $P(\lambda_{\min})$ are not fits but are obtained by rescaling such that $\langle \lambda_{\min} \rangle = 1$.) However, neither the ratio r nor the goodness-of-fit tests in Table I indicate that the chSE really provides a quantitative description of the data. The fact that the chSE seems to work better than the chUE should not be taken too seriously since neither of the two ensembles is supposed to be applicable in these cases. The apparent agreement of the shape of the curve with the chSE is, for all we know, purely accidental and should not be interpreted as a transition to symplectic symmetry.

We have also constructed $P(s)$ for the same parameter values that were used in Figs. 1 and 2. Two examples are shown in Fig. 3. In agreement with the observations of Ref. [2], we find that $P(s)$ is always described by the chUE prediction, even in those cases where $\rho(0)$ vanishes. This is consistent with the fact that, even in the chirally symmetric phase, the bulk spectral correlations of the Dirac operator are still described by RMT [9].

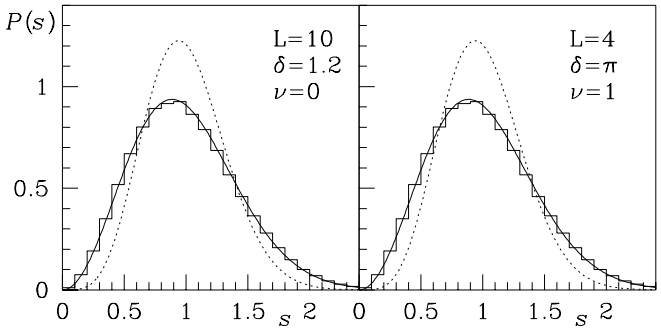

FIG. 3. Nearest neighbor spacing distribution $P(s)$ for some of the parameter values for which $P(\lambda_{\min})$ is not described by the chUE. The histogram represents the data, and the solid and dotted curves are the chUE and chSE predictions of Eq. (8), respectively.

V. CONCLUSIONS

Let us summarize the picture which has emerged from the study of the random matrix model. The Dirac operator of the Schwinger model has the symmetries of the chUE, and our model has the same symmetries, the only essential difference being the replacement of the U(1) gauge fields by random phases. The bulk spectral correlations of the Dirac operator, measured by $P(s)$, are described by the chUE result for all values of the parameters, regardless of whether or not $\rho(0)$ is nonzero. This is consistent with the findings of Ref. [2]. The microscopic spectral correlations, here measured by $P(\lambda_{\min})$, are given by the chUE predictions only for those values of the parameters for which $\rho(0) > 0$. By changing the parameters one can decrease the physical volume and cause $\rho(0)$ to vanish. The small eigenvalues are then no longer described by RMT. In this case, however, there exist some special values of the parameters for which the shape of the distribution of the smallest eigenvalue resembles that of the chSE. However, other measures such as the ratio r of Eq. (11) and the various goodness-of-fit tests clearly show that the chSE does not describe the data. Thus, the apparent agreement with the symplectic symmetry case is an artifact of chiral symmetry restoration in a finite volume and should be regarded as accidental.

There is a simple lesson to be learned from our analysis. If one wants to use random matrix methods to analyze data from lattice simulations, one has to make sure that one is working in a regime in which RMT is applicable. For the bulk spectral correlations, this is never really an issue. However, for RMT to describe the small Dirac eigenvalues it is necessary that $\rho(0) > 0$, i.e., that chiral symmetry is spontaneously broken.

ACKNOWLEDGMENTS

This work was supported by the Deutsche Forschungsgemeinschaft (DFG), the US Department of Energy (DOE), and the RIKEN BNL Research Center (RBRC). We would like to thank A. Schäfer for many stimulating discussions throughout the course of this study. We also thank the authors of Ref. [2] for helpful communication and M. Göckeler, J.J.M. Verbaarschot, and H.A. Weidenmüller for valuable comments.

[1] P.H. Ginsparg and K.G. Wilson, Phys. Rev. D **25**, 2649 (1982).
[2] F. Farchioni, I. Hip, C.B. Lang, and M. Wohlgenannt, Nucl. Phys. **B549**, 364 (1999).
[3] P. Hasenfratz, Nucl. Phys. **B525**, 401 (1998).
[4] H. Neuberger, Phys. Rev. D **57** 5417 (1998); Phys. Lett. **B 417**, 141 (1998), **B 427**, 353 (1998).
[5] T. Banks and A. Casher, Nucl. Phys. **B169**, 103 (1980).
[6] E.V. Shuryak and J.J.M. Verbaarschot, Nucl. Phys. **A560**, 306 (1993).
[7] J.J.M. Verbaarschot, Phys. Rev. Lett. **72**, 2531 (1994).
[8] M.L. Mehta, *Random matrices*, 2nd ed. (Academic Press, San Diego, 1991).
[9] R. Pullirsch, K. Rabitsch, T. Wettig, and H. Markum, Phys. Lett. **B 427**, 119 (1998).
[10] T. Wilke, T. Guhr, and T. Wettig, Phys. Rev. D **57**, 6486 (1998).
[11] M.E. Berbenni-Bitsch, S. Meyer, and T. Wettig, Phys. Rev. D **58**, 071502 (1998).
[12] P.J. Forrester, Nucl. Phys. **B402**, 709 (1993).
[13] W.T. Eadie et al., *Statistical Methods in Experimental Physics*, (North Holland, Amsterdam, 1971).
[14] W.H. Press et al., *Numerical Recipes* (Cambridge University Press, New York, 1986).